Stable Silicene in Graphene/Silicene Van der Waals Heterostructures

Geng Li, Lizhi Zhang, Wenyan Xu, Jinbo Pan, Shiru Song, Yi Zhang, Haitao Zhou, Yeliang Wang, Lihong Bao, Yu-Yang Zhang, Shixuan Du,* Min Ouyang, Sokrates T. Pantelides, and Hong-Jun Gao*

Silicene-based van der Waals heterostructures are theoretically predicted to have interesting physical properties, but their experimental fabrication has remained a challenge because of the easy oxidation of silicene in air. Here, the fabrication of graphene/silicene van der Waals heterostructures by silicon intercalation is reported. Density functional theory calculations show weak interactions between graphene and silicene layers, confirming the formation of van der Waals heterostructures. The heterostructures show no observable damage after air exposure for extended periods, indicating good air stability. The I–V characteristics of the vertical graphene/silicene/Ru heterostructures show rectification behavior.

As a 2D analog of graphene,[1,2] silicene has recently been the subject of extensive research interest.[3–13] Theoretical work has focused on the interesting physical properties of silicene. For example, it has been found that silicene possesses a band structure that is similar to that of graphene, with massless Dirac-fermion charge carriers.[4] An energy gap can be opened and tuned by either applying an external perpendicular electric field[8,9] or alkali-atom adsorption.[10] Also, silicene has pronounced spin–orbit coupling, which led to the prediction that the quantum spin-Hall effect[11] and the quantum anomalous Hall effect[12] would be detectable. In addition, silicene-based van der Waals heterostructures are predicted to have fascinating physical properties. The graphene-silicene vertical heterostructure is predicted to be a promising candidate as

anode material[14,15] and nanocapacitor,[16] and the silicene–arsenene vertical heterostructure is predicted to be useful in nanoelectronic and optoelectronic devices.[17]

On the other hand, the experimental fabrication of silicene-based devices remains substantially challenging because silicene itself is unstable in air.[18,19] A silicene field-effect transistor (FET) was recently fabricated by Tao et al. through a growth-transfer-fabrication approach.[13,20] A room-temperature mobility of ≈ 100 cm^2 V^{-1} s^{-1} was measured in their device, which, however, degraded in air after ≈ 2 min. Du et al. proposed another method to increase the chemical resistance of silicene to oxygen.[21] They fabricated bilayer silicene on Ag(111) and intercalated oxygen atoms which oxidized the bottom layer. While the stability of the top silicene layer improved, Raman data indicate extensive degradation of the sample in air after 120 h. Molle et al. successfully stabilized silicene by capping it with Al or Al$_2$O$_3$ film.[22] Silicene encapsulated between the capping layer and the metal substrate was shown to be stable in ambient conditions, but the existence of a few-nm-thick capping layer does not allow the fabrication of silicene-based heterostructures.

Moreover, silicene-based van der Waals heterostructures, which have been studied theoretically,[14–17] have not been experimentally demonstrated yet. Kiraly et al. deposited carbon and silicon on Ag(111) surface and found both lateral and vertical graphene-silicon heterostructures, but the Si atoms are sp^3-bonded as in bulk crystalline Si,[23] not silicene. De Crescenzi et al. demonstrated the growth of silicene nanosheets on a graphite surface in ultrahigh vacuum.[24] While the interaction between the silicene layer and the graphite was found to be van der Waals type, the structure would be unstable in air.

In this paper, we report the experimental fabrication of graphene/silicene van der Waals heterostructures. The graphene layer is grown first on a Ru(0001) substrate and silicene is constructed under it by Si intercalation. By controlling the amount of silicon, different types of silicene nanostructures are fabricated under graphene and imaged by scanning tunneling microscopy (STM). At low dosage, a periodic array of silicene-like patches under the atop regions of the graphene moiré pattern is a new type of intrinsically patterned[25] 2D material. At higher dosages, the intercalated Si forms a silicene monolayer. Covalent bonding between neighboring Si atoms in this silicene layer and weak interactions between graphene

Dr. G. Li, Dr. L. Z. Zhang, Dr. W. Y. Xu, Dr. J. B. Pan, Dr. S. R. Song, Dr. Y. Zhang, Dr. H. T. Zhou, Prof. Y. L. Wang, Prof. L. H. Bao, Prof. Y.-Y. Zhang, Prof. S. X. Du, Prof. H.-J. Gao
Institute of Physics and University of Chinese Academy of Sciences, and CAS Center for Excellence in Topological Quantum Computation
Chinese Academy of Sciences
Beijing 100190, China
E-mail: sxdu@iphy.ac.cn; hjgao@iphy.ac.cn
Dr. G. Li, Prof. M. Ouyang
Department of Physics
University of Maryland
MD 20742, USA
Prof. Y.-Y. Zhang, Prof. S. T. Pantelides
Department of Physics and Astronomy and Department of Electrical Engineering and Computer Science
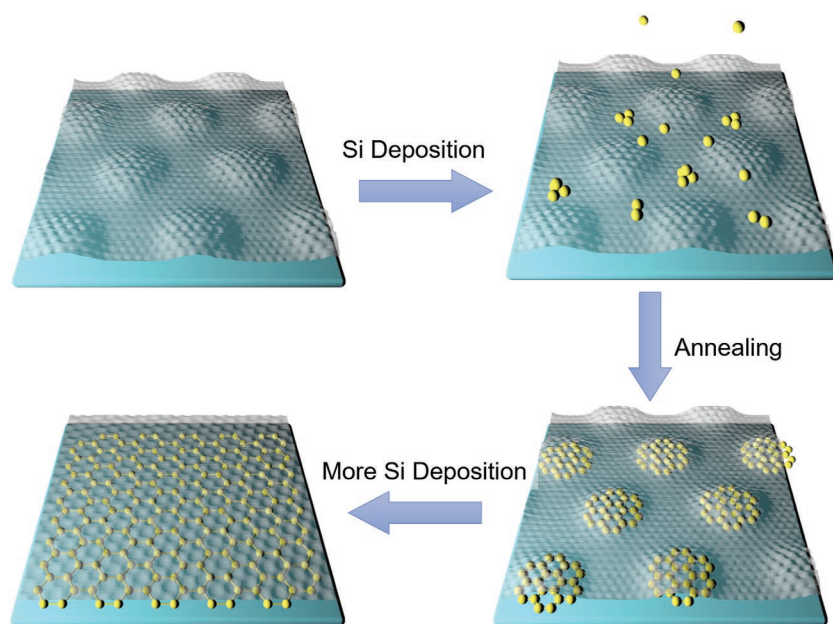Vanderbilt University
Nashville, TN 37235, USA

Figure 1. Schematic diagram of the formation of silicene structures at the graphene/Ru(0001) interface. The deposited Si atoms intercalate between graphene and the Ru substrate during annealing process. With a small Si dosage, Si atoms form honeycomb silicene nanoflakes below the atop regions. With more Si intercalation, silicene monolayers and multilayers form.

higher Si dosage, multilayer silicene forms between the graphene and the substrate. The as-prepared graphene/silicene heterostructures have been exposed in ambient conditions for two weeks and no observable damage was found. The vertical graphene/multilayer-silicene/Ru heterostructure shows rectification behavior with an ideality factor of ≈1.5. This work ushers the development of stable silicene-based devices.

Figure 1 illustrates the sequence of fabricating a graphene/silicene heterostructure. First, a graphene monolayer is epitaxially grown on a Ru(0001) substrate. Silicon atoms are then deposited on top and annealed at 900 K. This result in Si intercalation and the formation of silicene nanoflakes, monolayers, and multilayers, depending on the Si dosage (the amount of time the Si source is turned on). At each Si dosage, the samples are subsequently cooled down to 5 K for STM characterization.

Figure 2a shows a typical STM topography of a Si-intercalated sample for which the Si source was on for 5 min.[26–28] This small dosage of Si enables us to study the initial structure of the Si atoms intercalated between graphene and Ru(0001). The periodic pattern can be assigned to the moiré structure of graphene on Ru(0001).[26] However, compared with the moiré structure of graphene on Ru
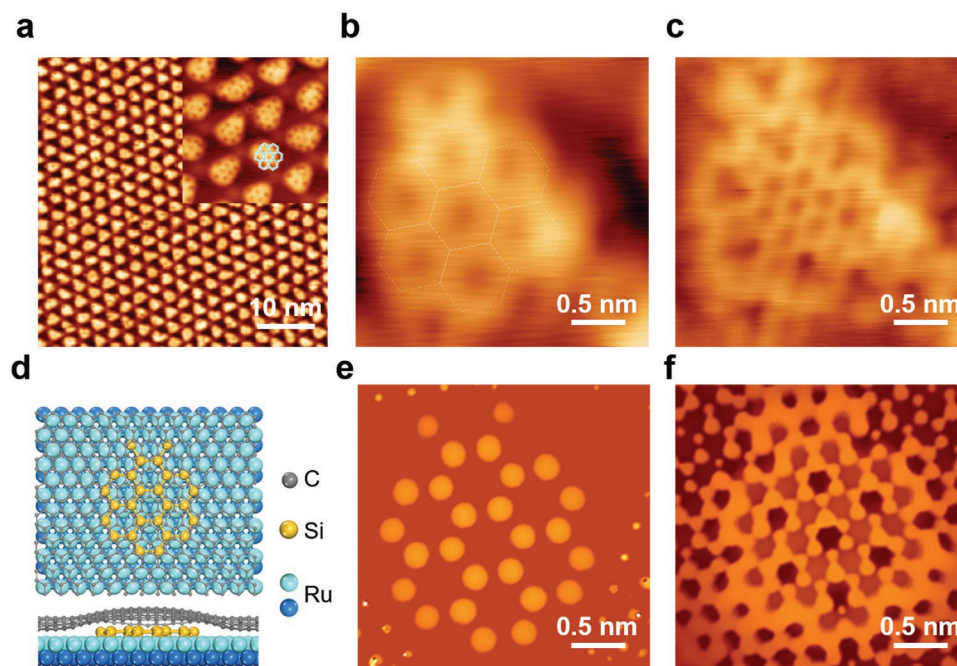
and silicene layers are confirmed by density functional theory (DFT) calculations, indicating that the fabricated structures are graphene/silicene van der Waals heterostructures. At even

Figure 2. Formation of silicene nanoflakes. a) STM topography showing the graphene/Ru(0001) structure after Si intercalation. Inset: zoom-in image of (a). b,c) Atomic-resolution images taken at the same area under different sample bias voltages (−0.5 V for (b) and −0.1 V for (c)). d) Proposed atomic model showing 26 Si atoms intercalated below the atop region. e,f) Simulated STM images of the configuration in (d) at different sample bias voltages (−0.5 V for (e) and −0.1 V for (f)).

without Si intercalation (Figure S1a, Supporting Information), expansion and distortion of the atop regions[29] can be clearly identified. The line profile analysis (Figure S1, Supporting Information) shows that the rippling of the moiré structure is ≈0.2 Å larger after Si intercalation, indicating a further corrugation of the graphene film along the direction perpendicular to the substrate surface. In addition, a zoom-in image of the intercalated sample (Figure 2a inset) reveals patches of a new honeycomb lattice with a nearest-neighbor distance of 2.67 ± 0.07 Å, which is significantly larger than the carbon–carbon distance in the graphene lattice. This new honeycomb lattice is never observed on a graphene/Ru(0001) sample without Si intercalation and has not been reported in previous works.[26,30] We can, therefore, safely conclude that the formation of the new honeycomb-lattice patches at the atop regions is related to the interfacial Si atoms. The periodic formation of the patches in effect results in a novel form of "intrinsically patterned" 2D materials in the sense of ref. [25].

Figure 2b,c shows the bias-dependent STM images acquired at the same area but under different sample bias voltages (−0.5 V for Figure 2b and −0.1 V for Figure 2c). Such bias-dependent images are fully reproducible with different tips and samples. Examination of Figure 2b,c clearly reveals the existence of two different periodicities in 30° rotation with respect to each other. The smaller honeycomb feature in Figure 2c exhibits a nearest-neighbor distance of ≈1.50 Å, which can be attributed to the intrinsic graphene lattice. This feature suggests that the graphene lattice remains intact in spite of the geometric change at the atop regions during the intercalation process. However, the larger honeycomb feature in Figure 2b shows a nearest-neighbor distance of ≈2.67 Å, which is larger than the C−C bonding length and can be attributed to the underlying silicon atoms. A Fourier-transformed image of Figure 2c clearly reveals the existence of the two sets of honeycomb lattices (Figure S2, Supporting Information).

An intuitive way of thinking about the emerging honeycomb pattern is that the Si atoms are confined below the atop regions, packing into honeycomb nanoflakes. Moreover, by employing the long-range periodicity of the moiré pattern of graphene as a template, a unique array of interfacial Si structures can be formed (Figure S3, Supporting Information). The lateral sizes of these flakes are uniformly distributed (≈15 Å) due to the confinement of the overlying strained graphene film.

To validate our interpretation of the experimental observations, we have performed DFT calculations. A supercell with 12 × 12 graphene on 11 × 11 Ru(0001) is used and the silicon atoms are placed between graphene and Ru(0001). We found that after six silicon atoms are intercalated, they preferentially stay below the atop site[29] and form a hexagon at the center (Figure S4, Supporting Information). Further incoming silicon atoms extend the hexagon into a honeycomb structure, with a rotation angle of 30° with respect to graphene (Figure S4, Supporting Information), which is consistent with the experimental observations. A typical relaxed structure of the atop region intercalated by 24 silicon atoms (with the geometry shown in Figure S4c, Supporting Information) reveals a stretched honeycomb structure with Si–Si distances of 2.62–2.87 Å, which matches well the STM results (≈2.67 Å). The DFT results also show that, at low coverage, these Si atoms tend to settle in registry

with the hexagonal Ru surface, leading to pseudomorphic honeycomb growth. Moreover, the calculations suggest that the preferential intercalation indeed results in an enhanced corrugation of 0.85 Å of the graphene film (Figure S5, Supporting Information). This corrugation is larger than the experimental value (≈0.2 Å) since the latter actually reflects the variation of the local density of states rather than the real height.

In order to reproduce the STM images in Figure 2b,c, we performed STM simulations for the model in Figure 2d. The results with a sample bias of −0.5 V (Figure 2e) and −0.1 V (Figure 2f) agree well with the experimental data, which further verifies the honeycomb arrangement of the intercalated Si atoms. We note that ruthenium silicide is known to form under certain experimental conditions. The formation of ruthenium silicide gives a shoulder-like feature in the X-ray photoelectron spectroscopy (XPS) spectrum of the Si 2p peak due to the existence of Ru−Si bonds.[31,32] We performed XPS measurements and observed a single peak of the Si 2p spectrum, indicating no ruthenium silicide formation in this experiment (Figure S6, Supporting Information). The shape and position of the Si 2p peak suggest that the intercalated silicon atoms in a G/Ru interface are in the elemental or zero-valence (unoxidized) state.[27,32] Therefore, we can safely conclude that the interfacial Si honeycomb structures observed here are silicene nanoflakes. Since both the silicene and graphene lattice can be resolved under different bias voltages, we found that nearest Si–Si distance (2.76 Å) is larger than the previously reported values (≈2.20 Å) as well as the value in bulk silicon (2.35 Å), which means that the silicene nanoflakes are stretched. The reason is that the Si atoms prefer to reside on top of the hollow sites of the Ru(0001) substrate, leading to the pseudomorphic growth of silicene nanoflakes. The pseudomorphic silicene nanoflake arrays can grow up to micrometer size (Figure S3, Supporting Information).

We have further observed that, under high Si dosage, the silicene nanoflake features disappear. After all the atop sites have been intercalated by Si atoms, further incoming Si atoms sequentially occupy the fcc and hcp sites, as has been demonstrated in a previous study,[30] and an intercalation-diffusion mechanism leads to formation of monolayer silicene. **Figure 3**a shows a typical sample obtained by supplying Si for 20 min. A new structure with a periodicity of ≈0.7 nm is clearly imaged and is attributed to the structure of the interfacial Si atoms. Figure 3b displays an atomic-resolution image of the carbon lattice, indicating that the graphene layer is intact. The nearest carbon–carbon distance is measured to be 1.41 Å, similar to the value in freestanding graphene,[2] indicating the decoupling of graphene from the Ru substrate.[26]

In order to determine the structure of the interfacial Si layer, we performed DFT calculations. Indeed, it is more complicated to experimentally resolve the Si atoms in monolayers. For example, in other epitaxial silicene systems, due to the buckling and probably reconstruction of silicene on the substrates, only a fraction of the Si atoms can be clearly identified by STM.[3,7,33] The silicene structure was determined by combining the STM images with DFT calculations, which is a well-established technique. Our DFT calculations show that the most stable structure of the interfacial Si is a full buckled silicene layer with a √3 × √3 superstructure on √7 × √7 Ru(0001), as shown in Figure 3c
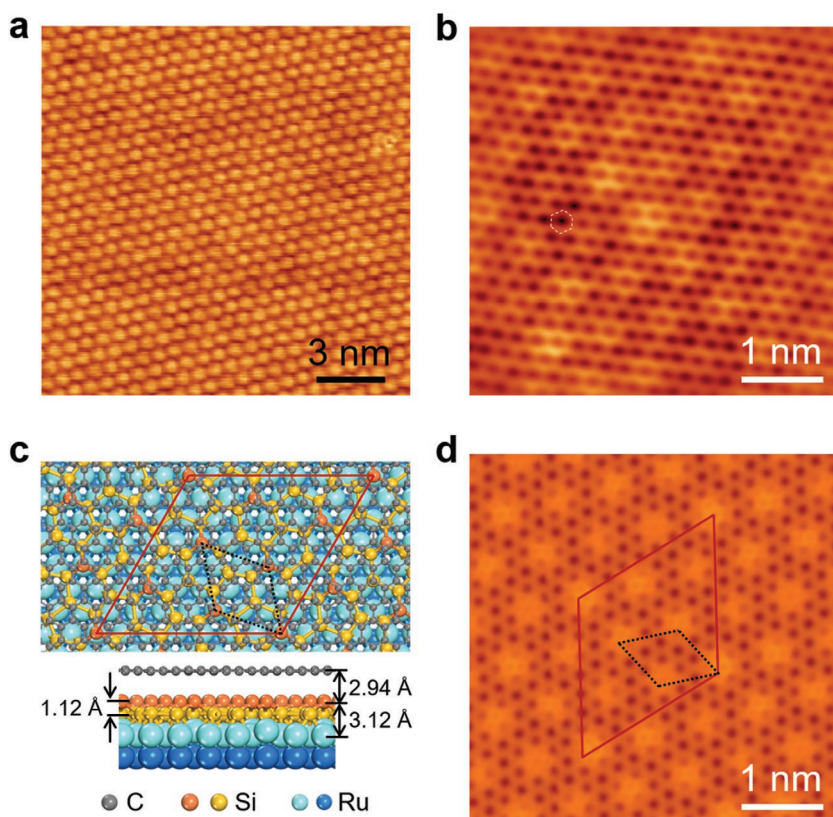
Figure 3. Formation of silicene monolayers. a) STM image of monolayer silicene encapsulated between graphene and Ru(0001). b) Atomic-resolution image showing intact carbon lattice. A hexagon is used to outline the honeycomb feature. The nearest carbon–carbon distance is measured to be 1.41 Å. Scale bar: 1 nm. c) Top and side views of the relaxed atomic model of the (7 × 7) Ru(0001)/($\sqrt{21} \times \sqrt{21}$) silicene/(8 × 8) graphene configuration (supercell is marked by a red rhombus). d) Simulated STM image for the configuration in (c).

(one supercell is marked by a dashed rhombus). A slightly distorted honeycomb Si lattice can be clearly recognized, with Si–Si distances ranging from 2.32 to 2.75 Å. While the honeycomb Si lattice cannot be directly differentiated in the STM image due to its buckled structure (bottom panel in Figure 3c), the $\sqrt{7} \times \sqrt{7}$ structure agrees well with the 0.7 nm periodicity, whereby each bright spot in Figure 3a corresponds to the location of a Si atom highlighted in orange in Figure 3c. The large distance (2.94 Å) between graphene and silicene suggests relatively weak interactions. In order to confirm our identification of the silicene structure and compare with the experimental images, an atomic model containing (7 × 7) Ru(0001)/ ($\sqrt{21} \times \sqrt{21}$) silicene/(8 × 8) graphene (supercell is marked by a red rhombus) is constructed and simulated. Figure 3d displays the STM simulation of the model, which reproduces the experimental data well.

DFT calculations show that both the nanoflake and monolayer silicene structures are grown in registry with the Ru substrate (Figure 2d, Figure S4, Supporting Information, and Figure 3c, respectively). In the case of the nanoflakes, intercalating Si atoms stay preferentially below the atop sites. The reason for this preferential adsorption behavior is because the spacing between the Ru substrate and the graphene layer at the atop site is larger and the energy required to insert Si

atoms beneath the atop site is lower compared with the fcc and hcp sites.[30] In the case of monolayers, Si atoms form the commensurate $\sqrt{3} \times \sqrt{3}$ superstructure on $\sqrt{7} \times \sqrt{7}$ Ru(0001) (Figure 3c). Therefore, in both cases, the graphene layer essentially plays no role in defining the silicene symmetry, which is consistent with the fact that graphene and silicene monolayers interact weakly.

If the Si dosage is further increased, bilayer or even multilayer silicene intercalated heterostructures form. When the number of layers of the intercalated silicene becomes larger than two, the graphene layer becomes flat and the moiré structure disappears,[26] which makes it difficult to analyze the underlying silicene structure by STM. We performed low energy electron diffraction (LEED) analysis to determine the structure of the multilayer silicene, as shown in Figure S7 (Supporting Information). We found that as the thickness of silicene increases, an attenuation in the intensity of the graphene/Ru(0001) moiré spots is observed, which is attributed to the decoupling of the graphene from the Ru substrate by the intercalated silicene layer. On the other hand, the $\sqrt{7} \times \sqrt{7}$ spots of silicene get brighter and sharper, indicating constructive addition of intensity from each layer. Therefore, the single-layer silicene is taken as a seed for successive overlayer growth, similar to the observation by Grazianetti et al. on multilayer silicene grown on Ag(111)/mica substrate.[34] We performed pertinent DFT calculations. The structures of the bilayer and multilayer silicene intercalated between graphene and Ru are shown in Figure S8 (Supporting Information). Both structures show a flat top Si layer, and a graphene/silicene distance of ≈3.5 Å, suggesting a van der Waals vertical stacking. We also calculated the projected density of states of multilayer silicene (Figure S9, Supporting Information) and found that, for more than five layers, except for the top two and bottom two layers, which are metallic, the middle layers exhibit a gap of only 0.2 eV compared with the calculated gap of 0.61 eV for bulk Si (the calculated values are underestimated because of the use of an approximate exchange functional). We conclude that multilayer silicene is distinct from bulk Si.

We have found that the silicene structures in Figures 2 and 3 are very stable. No observable damage or change of structure was observed even after exposure in air for extended periods, up to two weeks (Figure S10, Supporting Information). This result supports the notion that graphene in the fabricated heterostructure acts as a natural protection layer of silicene against air exposure. We note that capping with a single atomic layer enables ex situ characterization of silicene by means of surface analysis tools such as STM.

The interactions between graphene and silicene were investigated by calculating the electron localization function (ELF). The ELF has been demonstrated to be a useful tool to identify
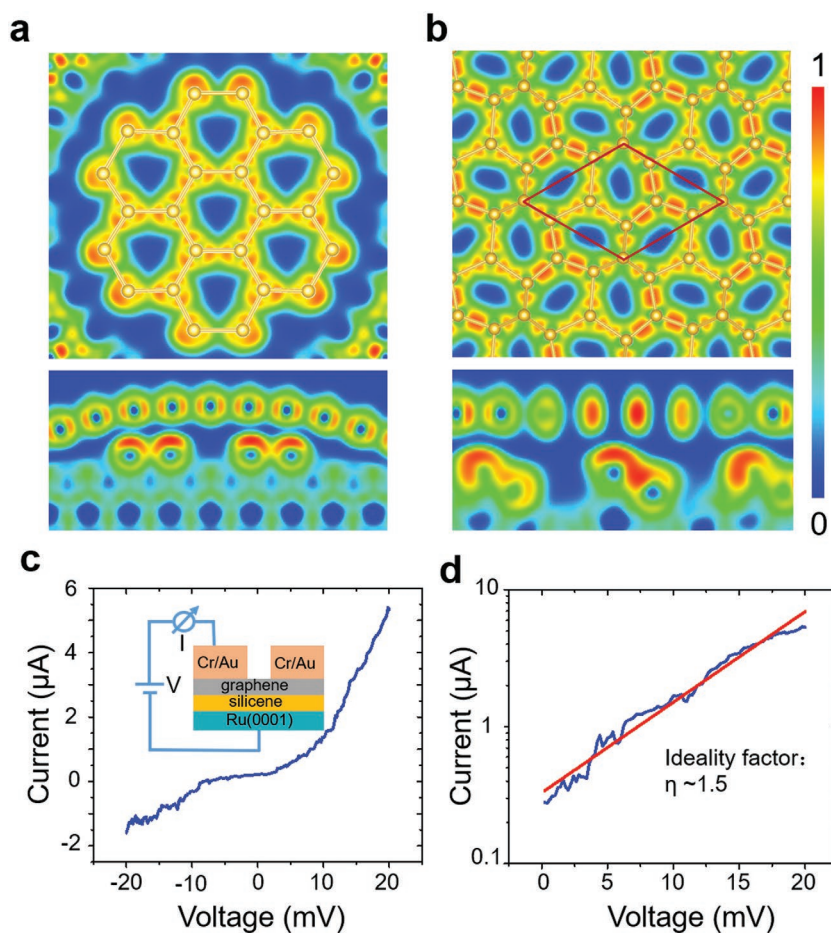
**ADVANCED
SCIENCE NEWS**

www.advancedsciencenews.com

**ADVANCED
MATERIALS**

www.advmat.de

Figure 4. ELF calculation and transport measurement of the graphene/silicene heterostructures. a,b) ELF maps of the pseudomorphic silicene nanoflake and monolayer at the plane of the Si atoms. Both the top view (upper panels) and side view (lower panels) images are shown. The unit cell of the monolayer structure is outlined by the rhombus. c) Current–voltage curve of a graphene/silicene/Ru vertical heterostructure measured at a temperature of 105 K, showing typical Schottky-like rectification behavior. Inset is a schematic diagram of the device structure and measurement setup. d) Logarithmic plot of the current–voltage curve. An ideality factor of ≈1.5 can be extracted by fitting it with Schockley's model.

of silicene is estimated to be ≈10 by taking account of both the Si dosage and intercalating cycles. Rectification is not observed in the case of graphene/monolayer-silicene/Ru heterostructure, most likely due to the strong bonding between monolayer silicene and the Ru substrate. The device structure, multilayer silicene intercalated between graphene and a Ru substrate, and its measurement setup are schematically shown in the inset of Figure 4c. Linearly fitting the logarithmic plot of the current–voltage curve based on Schockley's model, an ideality factor of ≈1.5 is extracted (Figure 4d), suggesting formation of a good interface between graphene and silicene. Measurements on the heterostructure at increasing temperatures show a trivial linear transport behavior since the elevated temperatures suppress the Schottky junction. It is worth noting that multilayer silicene FET device exhibits a characteristic ambipolar charge carrier transport behavior.[34] We also note that rectifying behavior at low temperature was previously predicted in a graphene/silicene bilayer heterostructure despite the metallic nature of the two materials.[14] For practical applications of this unique vertical heterostructure, further work, such as optimized device fabrication process and thickness control of silicene needs to be achieved.

In conclusion, by carefully controlling the intercalation process between Si and graphene, we have successfully achieved different types of silicon-based nanostructures: pseudomorphic silicene nanoflake arrays and continuous silicene monolayers and multilayers. Both experimental STM characterization and DFT simulations unambiguously support the identification of the observed structures. The interaction between graphene and silicene is similar to van der Waals layer heterostructures, as evidenced by an ELF study. The demonstrated air stability of these structures would be useful in future silicene device fabrication. Measurements on the vertical heterostructure indeed show a well-defined Schottky rectification behavior, suggesting that the as-grown graphene-silicene heterostructures represent an emerging class of stable and functional 2D heterostructures. We note that the fabricated heterostructures are still bonded to the metallic Ru substrate, which limit practical applications. Future research on transferring the heterostructures onto insulating substrates is necessary.

the chemical bonding strength from charge redistribution among atoms.[7] **Figure 4**a,b shows the ELF results for the pseudomorphic silicene nanoflake and the monolayer at the plane of the Si atoms. The ELF values between neighboring Si atoms are relatively large (0.63–0.75 for a nanoflake and 0.73–0.90 for monolayer silicene), suggesting the existence of covalent bonds between Si atoms. Cross-section images are also provided in the lower panels of Figure 4a,b where we can see that the ELF values are nearly zero between graphene and silicene. The low ELF values again verify the weak graphene–silicene interactions. This result suggests that the fabricated graphene-silicene structure is effectively a van der Waals heterostructure.

To demonstrate the potential application of this unique graphene/silicene/Ru heterostructure, we have measured the current–voltage characteristics of the graphene/multilayer-silicene/Ru heterostructure along the vertical direction at a temperature of 105 K and found a typical Schottky-like rectification behavior, as shown in Figure 4c. The layer number

Experimental Section

Sample Preparation: All experiments were performed in an Omicron low-temperature STM system equipped with a sample preparation chamber under a base pressure better than 1.0×10^{-10} mbar. Monolayer graphene was prepared by a well-developed technique through exposure of a Ru(0001) single-crystal surface to ethylene at 1300 K.[26] After that,

**ADVANCED
SCIENCE NEWS**
www.advancedsciencenews.com

**ADVANCED
MATERIALS**
www.advmat.de

Si atoms were deposited onto the surface at room temperature by running a current through a thin Si slice, followed by annealing at 900 K for the Si atoms to sufficiently intercalate. In order to characterize the growth process step by step, different amounts of Si were intercalated between graphene and the Ru(0001) substrate by varying the deposition time. The as-grown sample was transferred to a low-temperature STM chamber for characterization. All the STM images were acquired at 5 K.

DFT Calculation: Theoretical calculations were performed by using density functional theory as implemented in the Vienna ab initio simulation package (VASP)[35] with the projector augmented wave (PAW)[36] method. Local density approximation (LDA)[37] in the form of Perdew–Zunger was adopted for the exchange correlation potential. In the calculation, a vacuum layer of 15 Å was used and all Si atoms were relaxed until the net force on every atom is smaller than 0.01 eV Å^{-1}. The energy cutoff of the plane-wave basis set was 400 eV, and a single Γ point was employed for Brillouin zone integrations due to computational limitations. The LDA method gives an upper limit in evaluating the interactions between graphene and silicene.

Device Fabrication: Graphene/silicene/Ru vertical-heterostructure devices were fabricated using a standard e-beam lithography process and a metal stack of Cr/Au (5/50 nm) as contact electrodes. The *I–V* characteristics of the vertical heterostructures were measured in a home-designed four-probe UHV STM system with a cryostat using continuous liquid N_2 or He flow as cooling media. All electrical parameters were collected using a Keithley 4200 SCS system.

Supporting Information

Supporting Information is available from the Wiley Online Library or from the author.

Conflict of Interest

The authors declare no conflict of interest.

[1] K. S. Novoselov, A. K. Geim, S. V. Morozov, D. Jiang, Y. Zhang, S. V. Dubonos, I. V. Grigorieva, A. A. Firsov, *Science* **2004**, *306*, 666.
[2] A. H. Castro Neto, F. Guinea, N. M. R. Peres, K. S. Novoselov, A. K. Geim, *Rev. Mod. Phys.* **2009**, *81*, 109.
[3] P. Vogt, P. De Padova, C. Quaresima, J. Avila, E. Frantzeskakis, M. C. Asensio, A. Resta, B. Ealet, G. Le Lay, *Phys. Rev. Lett.* **2012**, *108*, 155501.
[4] L. Chen, C. C. Liu, B. J. Feng, X. Y. He, P. Cheng, Z. J. Ding, S. Meng, Y. G. Yao, K. H. Wu, *Phys. Rev. Lett.* **2012**, *109*, 056804.
[5] S. X. Sheng, J. B. Wu, X. Cong, W. B. Li, J. Gou, Q. Zhong, P. Cheng, P. H. Tan, L. Chen, K. H. Wu, *Phys. Rev. Lett.* **2017**, *119*, 196803.
[6] A. Fleurence, R. Friedlein, T. Ozaki, H. Kawai, Y. Wang, Y. Yamada-Takamura, *Phys. Rev. Lett.* **2012**, *108*, 245501.
[7] L. Meng, Y. L. Wang, L. Z. Zhang, S. X. Du, R. T. Wu, L. F. Li, Y. Zhang, G. Li, H. T. Zhou, W. A. Hofer, H. J. Gao, *Nano Lett.* **2013**, *13*, 685.
[8] Z. Y. Ni, Q. H. Liu, K. C. Tang, J. X. Zheng, J. Zhou, R. Qin, Z. X. Gao, D. P. Yu, J. Lu, *Nano Lett.* **2012**, *12*, 113.
[9] N. D. Drummond, V. Zolyomi, V. I. Fal'ko, *Phys. Rev. B* **2012**, *85*, 075423.
[10] R. G. Quhe, R. X. Fei, Q. H. Liu, J. X. Zheng, H. Li, C. Y. Xu, Z. Y. Ni, Y. Y. Wang, D. P. Yu, Z. X. Gao, J. Lu, *Sci. Rep.* **2012**, *2*, 853.
[11] C. C. Liu, W. X. Feng, Y. G. Yao, *Phys. Rev. Lett.* **2011**, *107*, 076802.
[12] M. Ezawa, *Phys. Rev. Lett.* **2012**, *109*, 055502.
[13] A. Molle, C. Grazianetti, L. Tao, D. Taneja, M. H. Alam, D. Akinwande, *Chem. Soc. Rev.* **2018**, *47*, 6370.
[14] X. F. Qian, Y. Y. Wang, W. B. Li, J. Lu, J. Li, *2D Mater.* **2015**, *2*, 032003.
[15] L. Shi, T. S. Zhao, A. Xu, J. B. Xu, *J. Mater. Chem. A* **2016**, *4*, 16377.
[16] F. Peymanirad, M. Neek-Amal, J. Beheshtian, F. M. Peeters, *Phys. Rev. B* **2015**, *92*, 155113.
[17] H. B. Shu, Y. L. Tong, J. Y. Guo, *Phys. Chem. Chem. Phys.* **2017**, *19*, 10644.
[18] A. K. Geim, I. V. Grigorieva, *Nature* **2013**, *499*, 419.
[19] G. Brumfiel, *Nature* **2013**, *495*, 152.
[20] L. Tao, E. Cinquanta, D. Chiappe, C. Grazianetti, M. Fanciulli, M. Dubey, A. Molle, D. Akinwande, *Nat. Nanotechnol.* **2015**, *10*, 227.
[21] Y. Du, J. C. Zhuang, J. O. Wang, Z. Li, H. Liu, J. Zhao, X. Xu, H. Feng, L. Chen, K. Wu, X. Wang, S. X. Dou, *Sci. Adv.* **2016**, *2*, e1600067.
[22] A. Molle, C. Grazianetti, D. Chiappe, E. Cinquanta, E. Cianci, G. Tallarida, M. Fanciulli, *Adv. Funct. Mater.* **2013**, *23*, 4340.
[23] B. Kiraly, A. J. Mannix, M. C. Hersam, N. P. Guisinger, *Chem. Mater.* **2015**, *27*, 6085.
[24] M. De Crescenzi, I. Berbezier, M. Scarselli, P. Castrucci, M. Abbarchi, A. Ronda, F. Jardali, J. Park, H. Vach, *ACS Nano* **2016**, *10*, 11163.
[25] X. Lin, J. C. Lu, Y. Shao, Y. Y. Zhang, X. Wu, J. B. Pan, L. Gao, S. Y. Zhu, K. Qian, Y. F. Zhang, D. L. Bao, L. F. Li, Y. Q. Wang, Z. L. Liu, J. T. Sun, T. Lei, C. Liu, J. O. Wang, K. Ibrahim, D. N. Leonard, W. Zhou, H. M. Guo, Y. L. Wang, S. X. Du, S. T. Pantelides, H. J. Gao, *Nat. Mater.* **2017**, *16*, 1209.
[26] J. H. Mao, L. Huang, Y. Pan, M. Gao, J. F. He, H. T. Zhou, H. M. Guo, Y. Tian, Q. Zou, L. Z. Zhang, H. G. Zhang, Y. L. Wang, S. X. Du, X. J. Zhou, A. H. Castro Neto, H. J. Gao, *Appl. Phys. Lett.* **2012**, *100*, 093101.
[27] Y. Cui, J. F. Gao, L. Jin, J. J. Zhao, D. L. Tan, Q. Fu, X. H. Bao, *Nano Res.* **2012**, *5*, 352.
[28] C. Xia, S. Watcharinyanon, A. A. Zakharov, R. Yakimova, L. Hultman, L. I. Johansson, C. Virojanadara, *Phys. Rev. B* **2012**, *85*, 045418.
[29] Y. Pan, H. G. Zhang, D. X. Shi, J. T. Sun, S. X. Du, F. Liu, H. J. Gao, *Adv. Mater.* **2009**, *21*, 2777.

[30] G. Li, H. T. Zhou, L. D. Pan, Y. Zhang, L. Huang, W. Y. Xu, S. X. Du, M. Ouyang, A. C. Ferrari, H. J. Gao, *J. Am. Chem. Soc.* **2015**, *137*, 7099.

[31] S. Lizzit, R. Larciprete, P. Lacovig, M. Dalmiglio, F. Orlando, A. Baraldi, L. Gammelgaard, L. Barreto, M. Bianchi, E. Perkins, P. Hofmann, *Nano Lett.* **2012**, *12*, 4503.

[32] L. Pasquali, N. Mahne, M. Montecchi, V. Mattarello, S. Nannarone, *J. Appl. Phys.* **2009**, *105*, 044304.

[33] L. Huang, Y. F. Zhang, Y. Y. Zhang, W. Y. Xu, Y. D. Que, E. Li, J. B. Pan, Y. L. Wang, Y. Q. Liu, S. X. Du, S. T. Pantelides, H. J. Gao, *Nano Lett.* **2017**, *17*, 1161.

[34] C. Grazianetti, E. Cinquanta, L. Tao, P. De Padova, C. Quaresima, C. Ottaviani, D. Akinwande, A. Molle, *ACS Nano* **2017**, *11*, 3376.

[35] G. Kresse, J. Furthmuller, *Phys. Rev. B* **1996**, *54*, 11169.

[36] P. E. Blochl, *Phys. Rev. B* **1994**, *50*, 17953.

[37] J. P. Perdew, A. Zunger, *Phys. Rev. B* **1981**, *23*, 5048.